Research Square

Preprints are preliminary reports that have not undergone peer review.
They should not be considered conclusive, used to inform clinical practice,
or referenced by the media as validated information.

Structure and Evolution of Storms within the Mesoscale Convective Systems over the Monsoon Core Zone using active Remote Sensing Observations

Manisha Tupsoundare

MANISHATUPSOUNDARE@GMAIL.COM

Indian Institute of Tropical Meteorology https://orcid.org/0000-0003-4904-5368

Sachin Deshpande

IITM: Indian Institute of Tropical Meteorology https://orcid.org/0000-0003-2872-154X

Zhe Feng

PNNL: Pacific Northwest National Laboratory

Subrata Kumar Das

IITM: Indian Institute of Tropical Meteorology

Medha Deshpande

IITM: Indian Institute of Tropical Meteorology

Ashruba Ghorpade

IITM: Indian Institute of Tropical Meteorology

Research Article

Keywords: MCS, Monsoon, Rainfall, Cloud tracking

Posted Date: June 30th, 2026

DOI: https://doi.org/10.21203/rs.3.rs-10116481/v1

License: This work is licensed under a Creative Commons Attribution 4.0 International License.
Read Full License

Structure and Evolution of Storms within the Mesoscale Convective Systems over the Monsoon Core Zone using active Remote Sensing Observations

Manisha Tupsoundare[1, 2], Sachin M. Deshpande[1,2,3, *], Zhe Feng[4], Subrata Kumar Das[1,2,3], Medha Deshpande[1,3], Ashruba Ghorpade[1,3]

[1]Atmospheric Research Testbed, Indian Institute of Tropical Meteorology, Pune-411008, Ministry of Earth Sciences

[2]Department of Atmospheric and Space Sciences, Savitribai Phule Pune University, Pune, India

[3]Academy of Scientific and Innovative Research (AcSIR), Ghaziabad, Uttar Pradesh, India.

[4]Atmospheric Sciences and Global Change Division, Pacific Northwest National Laboratory, Richland, WA, USA

[*]*Corresponding author: Sachin Deshpande (sachinmd@tropmet.res.in)*

Abstract:

Mesoscale convective systems (MCSs) dominate monsoon rainfall over central India, yet their storm scale (~10 km) structure and evolution are poorly constrained. This study examines the lifecycle, 3-D structure, and environmental controls of MCSs during June-September 2019 monsoon season using high-resolution ground radar and satellite observations. A Lagrangian cloud-tracking framework is used to identify and track MCSs, while radar-based classification resolves convective, stratiform, and anvil components. A total of 93 MCSs are detected, contributing to over 40% of seasonal rainfall. Most MCS propagate westward with a mean speed of ~9 m s^{-1}, strongly modulating rainfall distribution. Convective intensity peaks during the early stages of the MCS life cycle, characterized by deep convective cores and high echo-top heights. As systems evolve, stratiform and anvil regions expand and dominate spatial coverage and total rainfall production. While convection governs rainfall intensity, stratiform precipitation dominates total rainfall due to its larger spatial extent and persistence. Contoured frequency by altitude diagrams (CFADs) reveals distinct vertical structures among convective, stratiform, and anvil regions, reflecting their unique microphysical and dynamical characteristics. A pronounced diurnal cycle is observed, with afternoon peaks in convection followed by the growth of stratiform and anvil regions during mature stages. ERA5 vertical profiles further indicate that longer-lived MCSs and larger anvils form in environments with stronger deep-layer meridional shear and higher mid-level moisture favoring organized ascent and enhanced stratiform persistence. These results provide important observational constraints on monsoonal MCSs, embedded storm structures, and evolution, and serve as a benchmark for evaluating high-resolution numerical simulations of MCSs.

Keywords: MCS; Monsoon; Rainfall; Cloud tracking

1. Introduction

Atmospheric deep convection exists as both isolated convective storm or organized systems on mesoscale dimensions and plays a fundamental role in the global circulation and hydrological cycle. The largest and most organized form of deep convection is the MCSs, which accounts for a major fraction of total precipitation in the Tropics (e.g. Houze, 2004). MCSs form when convection aggregates and grows upscale, with interactions among individual storms producing organized mesoscale circulations (Houze, 2004). They typically span several hundred to thousands of kilometers in horizontal extent and can persist for up to 24 hours. Structurally, MCSs comprise intense convective cores embedded within extensive stratiform precipitation regions (Houze & Betts, 1981), distinguishing them from isolated thunderstorms. Numerous observational studies across different regions have demonstrated a broad universal structural organization of MCSs (e.g., Zipser, 1977; Houze & Betts, 1981; Houze & Mapes, 1991; Houze, 2004). MCSs contribute more than 50% of total tropical precipitation (Yuan & Houze, 2010), with contributions reaching up to 80% in some regions (Nesbitt et al., 2006; Roca et al., 2014). Over the Indian land (ocean) region, MCSs contribute approximately 40–60% (60–80%) of monsoon-season (JJAS) rainfall (Tupsoundare et al., 2025). A defining characteristic that separates MCSs from ordinary deep convection is their large proportion of stratiform precipitation (Houze, 1997; Schumacher & Houze, 2003; Liu et al., 2021), which produces a top-heavy latent heating profile (Schumacher et al., 2004; Liu et al., 2015). This top-heavy heating structure strongly influences large-scale circulation and atmospheric dynamics (Schumacher et al., 2004). In addition, MCSs are frequently associated with severe weather phenomena, including lightning, strong winds, hail, and flooding (Houze, 2004), often resulting in substantial societal and economic impacts (Doswell et al., 1996; Zipser et al., 2006; Feng et al., 2016; Houze, 2018; Hu et al., 2021). The lifecycle of an MCS typically includes initiation, mature, and dissipation stages, and systems are commonly classified into leading-line trailing-stratiform or disorganized types based on storm arrangement (Houze, 2004). During the mature stage, MCS consists of multiple intense convective cells or storms embedded within an extensive anvil cloud shield formed by interacting cumulonimbus clouds (Houze, 1989; Sindhu & Bhat, 2018). Individual convective storms are much smaller in scale than MCSs and generally persist for less than one hour, with only a small fraction lasting longer than one hour (Dixon, 1993; Shah et al., 2015) and very few exceeding three hours (Davini et al., 2012; Sindhu & Bhat, 2019). These storms fall within scale C ($1–10^2$ km^2) and scale D ($10^2–10^3$ km^2) categories of atmospheric systems (Houze, 1977). Despite their smaller size, storm-scale convection contributes approximately 90–97% of total convective precipitation, underscoring the importance of understanding storm characteristics for both scientific and practical applications (Sindhu & Bhat, 2018). Studying storms embedded within MCSs is particularly important because these storms represent the fundamental building blocks of the larger convective system. While MCSs determine the overall precipitation pattern and mesoscale circulation. Individual storms control the

spatial distribution, intensity, and temporal evolution of rainfall through variations in convective core structure and organization (Rowe et al., 2012; Schiro et al., 2020). Embedded storms influence the development of stratiform regions and contribute to MCS organization by generating cold pool outflows and associated mesoscale convergence (Houze, 2004). Understanding storm-scale processes is therefore essential for improving numerical weather prediction and nowcasting, as convective-scale features are often poorly represented in models. Linking storm-scale dynamics to MCS evolution enables more accurate quantification of individual storm contributions to total precipitation, improved assessment of localized weather hazards, and clearer understanding of feedback between convective and mesoscale circulations. MCSs have been extensively studied worldwide (e.g., Zipser, 1977; Houze & Betts, 1981; Houze & Mapes, 1991; Houze, 2004; Houze et al., 2015; Feng, et al., 2018; Feng et al., 2019), fewer studies have examined storm-scale characteristics using ground-based radar observations (e.g., Lopez, 1976; Cetrone & Houze, 2006; Potts et al., 2000; Davini et al., 2011; Goudenhoofdt & Delobbe, 2013; Novo et al., 2013; Shah et al., 2015; Lang et al., 2007; May & Ballinger, 2007). Over India, storm-scale studies remain particularly limited (Resmi et al., 2015; Utsav et al., 2017; Sindhu & Bhat, 2018; 2019; 2021). Most previous investigations have relied on satellite observations to examine convective storm structure and evolution (Pokhrel & Sikka, 2013; Kumar & Bhat, 2016; Mangla et al., 2020; Tupsoundare et al., 2025), whereas only a few studies have utilized ground-based radar data (Deshpande et al., 2015; Das et al., 2021; Doyle et al., 2021; Krishna et al., 2021; Jha et al., 2023; Sindhu & Bhat, 2021; Utsav et al., 2017). One of the few studies addressing this linkage is (Rowe et al., 2012), who identified and tracked individual convective cells embedded within MCSs and examined their interaction with both isolated and organized convection. Consequently, how does storm-scale convection interact with MCS evolution, particularly in terms of the spatial and temporal evolution of storms within an MCS and their relationship with different stages of the MCS life cycle? In particular, what is the role of individual storms in contributing to total precipitation throughout their life cycle? How do they interact with isolated and organized convection, and how is their vertical structure represented within MCSs? These aspects remain inadequately documented in previous studies, highlighting the need for improved characterization of storm-scale processes within MCSs to better understand their evolution and associated precipitation characteristics. The present study addresses this gap by analysing MCSs observed within the Indian Monsoon Zone (MZ). The MZ, extending between 15°–25°N and 75°–91°E and encompassing Central India and the northern Bay of Bengal, is a critical component of the regional monsoon system. During the summer monsoon, the monsoon trough over Central India aligns with the continental tropical convergence zone, and precipitation is frequently associated with synoptic-scale disturbances such as monsoon lows and depressions originating over the Bay of Bengal and propagating northwestward (Rajeevan et al., 2010). These synoptic-scale systems play a key role in triggering MCSs and contribute substantially to both mean and extreme rainfall over the region (Phadtare & Bhat, 2019). As

a result, deep convection is frequent over Central India, where rainfall is vital for agriculture and water resources. Doppler Weather Radar (DWR) provides a powerful tool for observing the three-dimensional structure of convective systems with high temporal resolution, typically completing volume scans every 10 minutes. These observations enable continuous monitoring of storm evolution and precipitation characteristics over a wide spatial domain, facilitating detailed analyses of rainfall characteristics. Given the prevalence and multi-scale complexity of convection in the tropics, these observational capabilities are particularly valuable for applications such as nowcasting, short-term rainfall forecasting, and early flood warning systems. In this study, radar observations from the S-band DWR installed at Bhopal (23.24°N, 77.42°E; ~570 m above mean sea level) are used to examine the three-dimensional structure of storms embedded within MCSs during the 2019 monsoon season (JJAS). Figure 1 shows the topography of India and the radar location.

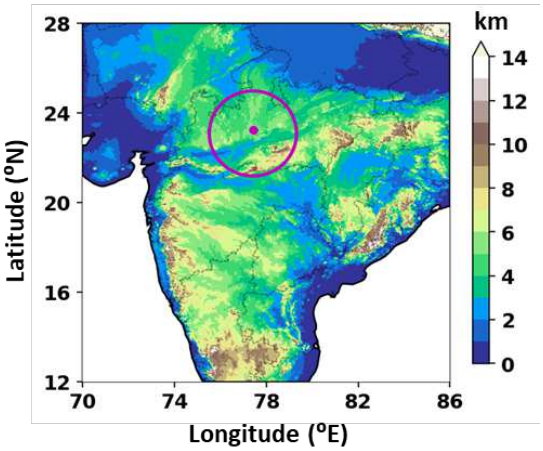


Figure 1. Topographic map of India derived from USGS global 30-arc-second terrain elevation data, showing the location of the IMD S band Doppler weather radar. The magenta dot indicates the S-band radar location, and the magenta circle represents the radar coverage range.

2. Data and analysis methods

2.1. Observational datasets

This study utilizes three high resolution observational datasets to investigate the characteristics, evolution, and internal structures of MCSs and their embedded storms in the core monsoon zone. Deep convective systems (DCSs) associated with MCSs are first identified using NOAA's global merged geostationary satellite 11.5-μm infrared brightness temperature (Tb) at 4 km spatial resolution (Janowiak et al., 2017). To characterize precipitation associated with these systems, we use Version 06B of the GPM IMERG surface precipitation dataset (Huffman et al., 2019). Three-dimensional (3D) structural features of MCSs are derived from S-band DWR radar reflectivity data obtained from the India Meteorological Department

(IMD) at Bhopal. The radar operates at a wavelength of 10.76 cm (frequency of 2.788 GHz) with a beam width of 0.93° and performs volumetric scans at elevation angles of 0.05°, 0.8°, 1.34°, 2.25°, 3.84°, 5.33°, 8.31°, 10.83°, 14.83°, and 20.4°. Radar volume scan data, available at 10-min intervals and originally recorded in a spherical polar coordinate system, are converted into three-dimensional Cartesian grids using the Radx algorithm (Dixon, 2014). The resulting dataset consists of 40 vertical levels with 0.5 km vertical resolution and a horizontal grid spacing of 1 km × 1 km, providing a uniform framework for subsequent three-dimensional analysis. For the 2019 Indian summer monsoon season (June–September), the processed radar data are used to examine the 3D morphology within MCSs. For integrated analysis, the satellite-based Tb and IMERG precipitation data are regridded to a common 1-km spatial grid to match the radar dataset. All datasets are further combined to an hourly temporal resolution for MCS tracking, which is sufficient to capture the lifecycle of large convective systems (Feng et al., 2019).

2.2. MCS Identification and Tracking

This study adopts the open-source Python FLEXible object TRacKeR (PyFLEXTRKR) method (Feng et al., 2023) to identify and track MCS. The tracking procedure is initiated using NOAA's global merged geostationary satellite infrared brightness temperature (Tb) data. Deep convective systems (DCSs) are first identified as cold cloud systems (CCSs) defined by a Tb threshold of 241 K, representing deep which corresponds to deep convective cloud tops typically associated with vigorous convection and widespread precipitation systems in the tropics. Contiguous cloud regions satisfying this threshold are labeled as CCS objects and tracked in time using an overlap-based tracking algorithm, which links cloud features between consecutive time steps based on spatial continuity. To ensure that the identified systems represent organized precipitating convection, CCSs are further constrained using precipitation and radar-based criteria. Precipitation features (PFs) are defined as contiguous regions with rain rates exceeding 1 mm h^{-1}, from IMERG data. The overlap between CCSs and PFs ensures that the identified cloud systems are associated with surface precipitation. Convective cores are identified using radar reflectivity data, whereas CCS size is determined independently from satellite infrared observations. An MCS is defined based on a combination of cloud, precipitation, and radar reflectivity characteristics. Specifically, a system is classified as an MCS if it satisfies the following criteria:

(i) CCS area > 20 × 10^3 km^2,

(ii) presence of an associated PF with a major-axis length exceeding 100 km,

(iii) existence of convective cores with radar reflectivity greater than 40 dBZ at any vertical level,

(iv) lifetime of at least 2 hours.

These thresholds ensure that only large, long-lived, and organized convective systems are considered consistent with previous studies (e.g., Feng et al., 2019, 2023). The temporal evolution of each identified MCS is tracked throughout its initiation, mature, and dissipation stages, and system propagation characteristics, including motion speed and direction, are estimated from the displacement of the CCS centroid between successive time steps.

3. Results and Discussion

3.1 Radar identified 3D structures and evolution of storms embedded in MCSs

An illustrative example of an observed MCS and its tracked evolution, including system trajectory, cloud-top brightness temperature, and associated precipitation, is shown in Figure 2. This MCS (lasting 22 hr) was triggered at 1030 LT on 08 August 2019 (LT; local time is UTC + 5.3 hr in India). Convection took around 6 hr to intensify into an MCS [we utilized a proxy for convective strength, the lowest IR *Tb*, which is related to the deepest cloud-top height]. Figure 2b shows the large extent of tall cloud top heights during the MCS mature phase that coincides with widespread heavy precipitation (Figure 2c).

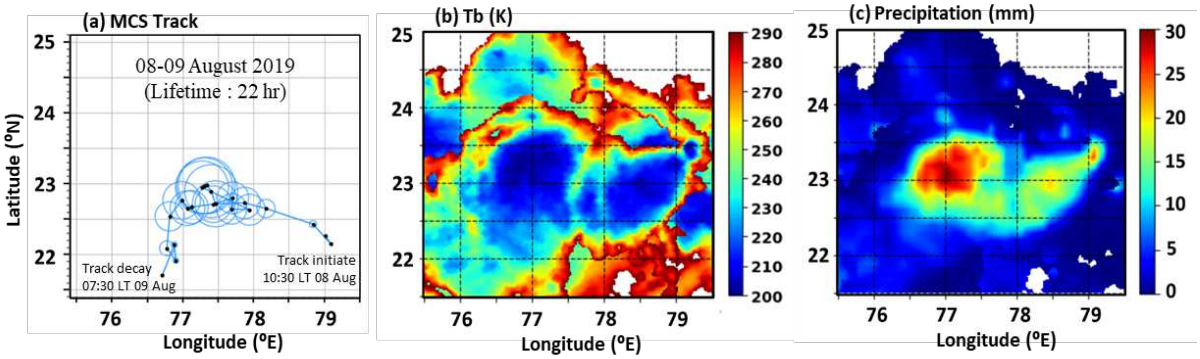


Figure 2: An illustration of an observed MCS that the tracking method detected and tracked during 1030 LT 08 August–0730 LT 09 August 2019. (a) An MCS track, with each circle, indicating a normalized MCS area at a specific hour throughout its lifetime. (b) Snaps of cloud top brightness temperature at various times during MCS lifetime, (c) snaps of accumulated rain at various times during MCS lifetime.

The internal convective structures of MCSs are analyzed using Bhopal S-band radar reflectivity data, which are classified into convective, stratiform, and anvil regions based on horizontal reflectivity gradients, echo intensity peakedness, and the vertical structure of radar echoes (Feng et al., 2011). Convective regions are characterized by intense, vertically developed radar echoes associated with intense precipitation and echo

tops exceeding 6 km. Stratiform regions exhibit more uniform and widespread precipitation with weak horizontal reflectivity gradients and occasionally, enhanced reflectivity near the melting layer, also maintaining echo tops above 6 km. Anvil regions represent the non-convective cloud shield and include transitional anvils (echo base < 3 km and echo top > 6 km), thick anvils (echo base > 3 km), and thin anvils, which are detected by satellite but not by radar. This classification enables the characterization of MCS structural evolution, including variations in convective, stratiform, and anvil regions throughout the storm lifecycle.

3.2 Storm structure identified by Radar data

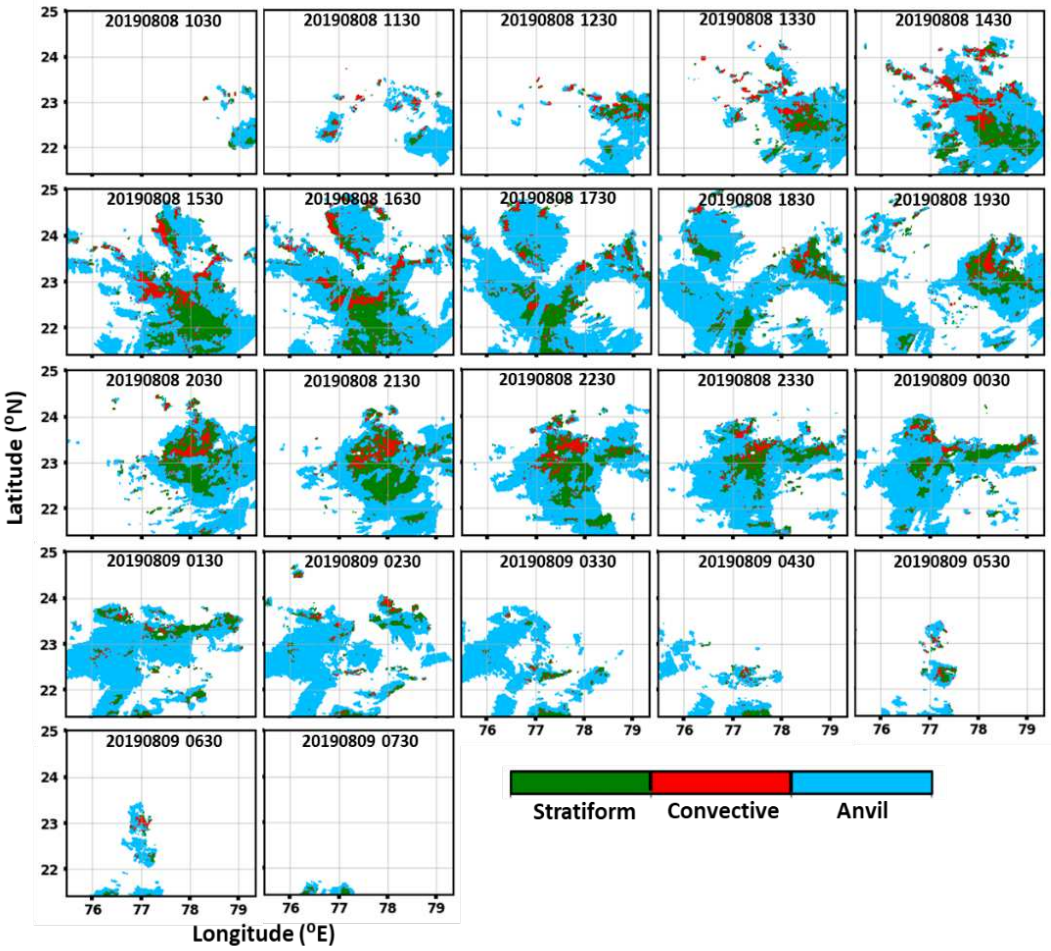


Figure 3. The life cycle of a convective system that is tracked in the study domain. Time increases from left to right, and each panel represents an hour. The colors represent cloud type regions identified by the classification scheme.

The spatial manifestation of the MCS lifecycle, showing the hourly evolution of a long-lived MCS tracked on 08–09 August 2019 across the study domain and highlighting how changes in cloud type and organization accompany its development, maturity, and decay, is illustrated in Figure 3. The developing stage extends until the minimum IR brightness temperature is reached, the mature stage spans the period from minimum IR temperature to maximum equivalent radius, and the dissipating stage begins once the system starts decreasing in size (Futyan & Del Genio, 2007). Convective (red), stratiform (green), and anvil (blue) regions are identified using the cloud classification scheme. The anvil category here includes all three subtypes transitional, mixed, and ice anvils. This classification enables clear visualization of the evolving mesoscale structure and cloud type transitions throughout the MCS lifecycle (Figure 3b). The system was initially detected at 1030 LT on 08 August 2019 over the southeastern part of the domain near 22.27° N and 79.02° E and subsequently expanded to horizontal extent as it propagated northwestward. During this early stage of development, convection appears as isolated small cells near the initiation region. In the following hours, the convective elements become spatially distributed as the system propagates northwestward, gradually embedded within expanding stratiform and anvil regions, indicating increasing spatial coherence of the MCS. By 1430 LT, a distinct convective segment separated from the northern flank of the main system, forming a smaller, short-lived convective feature. This secondary system dissipated by 2030 LT, while the main MCS maintained its structural coherence and continued propagating across the domain.

The MCS system reached its mature stage between 1530 and 2030 LT on 08 August, exhibiting a well-organized squall-line structure observed at 1530 and 1630 LT. This configuration consisted of a leading convective line, followed by a trailing stratiform region, and an expansive anvil cloud shield, all of which are characteristic features of a dynamically mature MCS. Such structural organization is typically associated with environments characterized by strong vertical wind shear and mesoscale lifting mechanisms, including the interactions between the cold pool and wind shear, which likely contributed to the system's longevity and sustaining its organized structure (Moncrieff, 1992; Parker & Johnson, 2000; Houze, 2004). Following the mature stage, the system began to decay gradually, with weakening convection and reduction in stratiform and anvil cloud coverage. By 0130 LT on 09 August, the convective activity had shifted southward, indicating a gradual propagation and structural evolution of the system. The dissipation phase was marked by a further reduction in intensity, with only weak convective echoes observed near the southwestern edge of the domain. The MCS was no longer detectable by 0730 LT on 09 August, completing a total life cycle of approximately 22 hours. Next, a detailed radar-based view of the internal horizontal and vertical structure of the system during its mature stage, offering insight into the dynamical and microphysical characteristics underlying its organized convection, is shown in Figure 4.

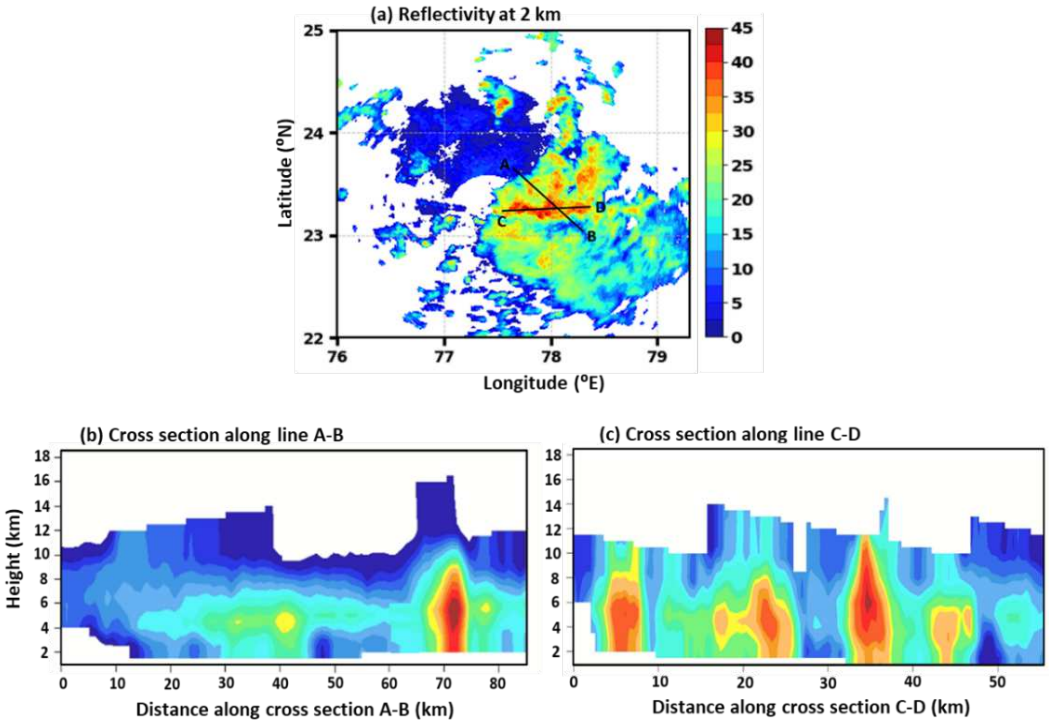


Figure 4. *Panel (a) shows radar reflectivity snapshot at 2 km altitude during mature stage of MCS at 1630 LT on 08 August 2019, Panel (b) and (c) show a vertical cross-section along line A-B and C-D, respectively.*

Figure 4 illustrates the instantaneous horizontal reflectivity structure of a mature convective cloud system at 1630 LT on 08 August 2019, highlighting the extensive spatial coverage and complex internal organization of the MCS. This system spans a large area, featuring multiple convective clusters with varying vertical extents, with the tallest cloud tops reaching altitudes of approximately 14 to 16 km. This radar snapshot corresponds to the mature phase identified in Figures 2, when the system exhibited maximum organization and convective intensity. The mature MCS is characterized by a pronounced squall line, consisting of a well-defined leading convective line followed by a trailing stratiform precipitation region, a classic signature of organized MCS. The vertical cross-sections along the marked transects (Figures 3b and 3c) reveal key aspects of the vertical structure of the convective system. The leading convective line exhibits a 10 dBZ echo top reaching heights of up to 13-15 km, indicative of strong and deep updrafts capable of lifting hydrometeors. Within this convective line, intense reflectivity cores exceeding 40 dBZ are observed between 7 and 8 km altitude (Kumar & Bhat, 2017), suggesting the presence of heavy precipitation particles such as graupel and hail. These high reflectivity values indicate active mixed-phase microphysical processes and substantial latent heat release, which contribute to the maintenance and intensification of deep convection. The presence of multiple such cells within the system shows that the

MCS was well-organized and capable of sustaining vigorous convection throughout its mature phase. During this period, the system demonstrates significant rainfall production, with estimated rain rates of approximately 11 mm/hr, covering a horizontal area exceeding 1.7×10^6 km². Such rainfall intensities and spatial coverage are characteristic of mature MCS (Houze, 2004). The combined horizontal and vertical radar structure of this MCS reflects the complexity and intensity of convective processes operating within the MCS, including deep convection, hydrometeor growth, and stratiform precipitation formation, all of which play a critical role in regulating the system's rainfall production and longevity (Houze, 1993; Zipser, 1994). To further illustrate the temporal evolution and lifecycle characteristics of such systems, an example of a long-lived MCS tracked over the radar domain is presented in Figure 5.

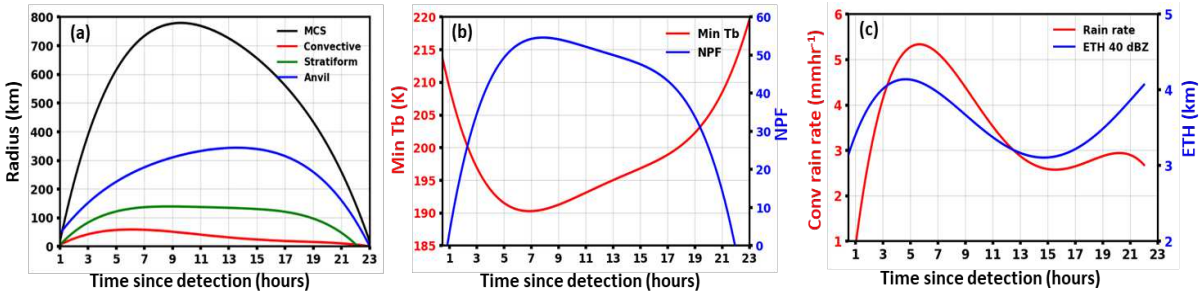


Figure 5. Example of the evolution of a tracked MCS showing (a) radius of the MCS (black line), and radii of convective (red), stratiform (green), and anvil clouds (blue); (b) minimum IR brightness temperature and number of precipitation features (NPFs); and (c) convective rain rate and 40 dBZ echo-top height. Lines represent fourth-order polynomial fits to the observed data.

The lifecycle and associated cloud and precipitation characteristics of a long-lived MCS are illustrated using satellite and radar observations. Following the initiation, the system required approximately 7–8 hours to undergo upscale convective growth, after which it reached its mature phase. This MCS exhibits a typical pattern of evolution of cloud and precipitation properties, progressing from its convective initiation to the mature and dissipation phases (Futyan & Del Genio, 2007). The developing stage extends until the minimum IR brightness temperature is reached, the mature stage spans the period from minimum IR temperature to maximum equivalent radius, and the dissipating stage begins once the system starts decreasing in size. As shown in Figure 5a, the equivalent radius of the MCS expanded rapidly following initiation and reached a maximum approximately 8 hours later, marking the mature phase of the system. Thereafter, the radius gradually decreased as the system weakened and decayed. The number of Precipitation Features (NPFs), defined as contiguous regions within the CCS producing rain rate exceeding

2 mm h^{-1}, peaked slightly earlier than the radius (Figure 5b). This temporal offset suggests that intense convective development and precipitation organization occurred during the early stage, prior to the maximum spatial extent of the system. The early peak in NPFs is indicative of rapid convective clustering and precipitation intensification during the formative phase of the MCS.

The convective cloud area (Figure 5a) increased rapidly during the initial development stage and reached its maximum coincident with the minimum infrared (IR) brightness temperature (Figure 5b), signifying presence of deep, vigorous convection with strong updraft activity. Subsequently, the convective area decreased gradually during the mature and dissipation phases. In contrast, both stratiform and anvil cloud areas increased substantially as the system developed. The stratiform region reached its maximum extent before the mature phase and declined sharply during dissipation, whereas the anvil cloud area continued to expand slightly beyond the convective peak and attained its maximum closer to the end of the mature phase before decreasing. This temporal lag between the peaks of convective and stratiform/anvil areas reflects the typical transition of an MCS from a convective to a more stratiform-dominated structure, with detrainment of hydrometeors playing a key role in the formation of an extensive anvil shield. The similar temporal trends in stratiform and anvil cloud coverage suggest their interconnected formation through detrainment and upper-level outflow from deep convection. As shown in Figure 5b, the minimum IR brightness temperature decreased rapidly during the early stages of development, consistent with increasing cloud-top heights and strengthening updrafts. The subsequent gradual warming of IR temperatures during later stages reflects progressive weakening of deep convection and the transition toward stratiform-dominated precipitation processes (Houze 1993, Houze, 2004). Figure 5c presents the evolution of convective rain rate and 40 dBZ echo top height, both of which serve as key indicators of connective strength. These two variables peaked during the late development to early mature stage, followed by a gradual decline during dissipation. The 40 dBZ echo top height, often associated with vigorous updrafts and large hydrometeors, provides a radar-based proxy for storm intensity and is consistent with the timing of deepest convection. Consistent with the behavior of the 40 dBZ echo top height, the convective rain rate increased during storm intensification and reached maximum values during peak convective activity.

3.3 Characteristics of MCS over radar domain

This section presents a comprehensive analysis of all MCSs identified and tracked over the radar domain during the JJAS period of 2019. Key physical properties of these MCSs include their frequency of occurrence, spatial extent, intensity, lifetime, propagation speed and direction, as well as associated precipitation characteristics are examined in detail.

3.3.1 Spatial distribution of MCS

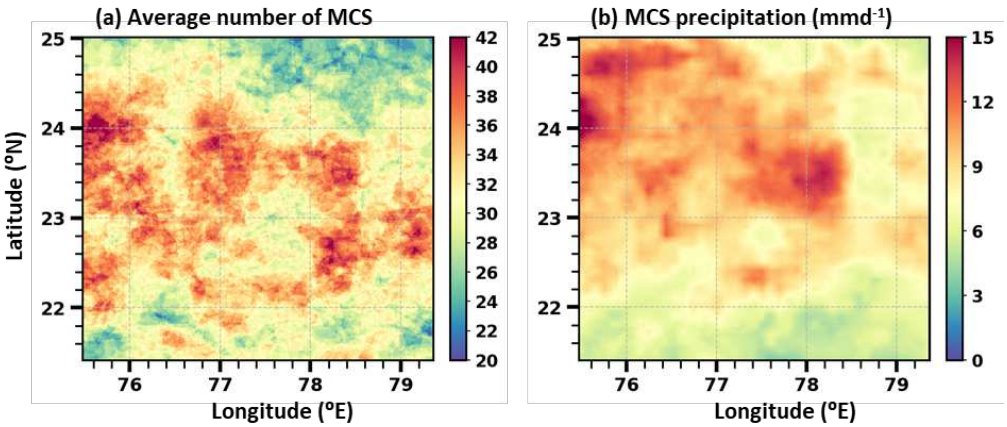


Figure 6: The Spatial distributions of (a) average MCSs initiation occurrence and (b) MCS precipitation (mm day^{-1}) during JJAS 2019 over radar domain.

The spatial distribution of MCS identified and tracked across the S-band DWR coverage area during the JJAS 2019 period is presented in Figure 6. A total of 93 MCSs were identified and tracked during the study period within the coverage area. These systems exhibit wide range of lifetimes, from short-lived to long-lived events, with many persisting for several hours and traveling hundreds of kilometers throughout their lifecycle. The spatial extent and longevity of these MCSs highlight their significant role in modulating regional precipitation patterns and the local precipitation budget via latent heat release, consistent with findings by (Yang & Majda, 2017; Yang et al., 2023). The initiation of MCSs is observed predominantly in the eastern and western parts of the domain, while fewer systems originate further north, indicating preferred regions for convective development likely influenced by mesoscale environmental conditions. The spatial distribution of average MCS occurrence (Figure 6a) closely mirrors the spatial pattern of MCS-related precipitation accumulation (Figure 6b). This clear connection shows that how often MCSs pass over a place strongly influences how much rain that area gets, highlighting the important role of MCSs in bringing monsoon rainfall to the region. Quantitatively, MCSs contribute more than 40% of the total precipitation during the monsoon season, underscoring their critical role in the regional hydrological cycle and associated water resources. Such dominance is consistent with other tropical regions where organized convective systems are primary drivers of seasonal rainfall (e.g., (Houze, 2004; Mapes et al., 2006). The observed spatial variability in MCS occurrence and precipitation suggests that their genesis, movement, and evolution are influenced by a combination of large-scale synoptic patterns and local thermodynamic conditions. Understanding these spatial characteristics is essential for improving regional precipitation forecasts and water management strategies under current and future climate conditions.

3.3.2 MCS propagation speed and direction

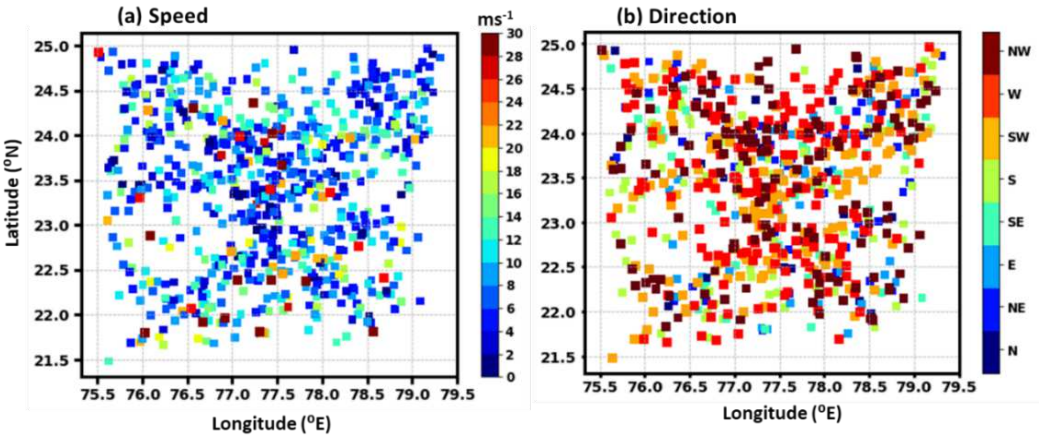


Figure 7: Spatial distribution of (a) Propagation speed of MCS and (b) Propagation direction of MCS over the study domain during JJAS 2029.

Building on the spatial occurrence and precipitation patterns discussed in section 3.3.1, the propagation characteristics of MCSs provide critical insights into how these systems influence the regional distribution and intensity of monsoon rainfall. The propagation speed and direction of MCSs play a crucial role in determining their overall impact, particularly regarding their lifespan, rainfall accumulation, and potential for generating hazardous weather, including damaging surface winds (Coniglio et al., 2006). Slow-moving MCSs, for instance, can remain over a particular location for extended periods, significantly increasing the risk of localized flooding due to prolonged rainfall. On the other hand, faster-moving systems may tend to affect large areas quickly, influencing broader regions but with potentially less rainfall accumulation at any single location. Figure 7a and 7b show the spatial distribution of propagation speed and direction for all tracked MCSs over the radar domain during the JJAS 2019 season. The propagation characteristics were estimated based on the centroid displacement over the lifetime of each MCS. The overall mean propagation speed across all systems is 9.1 m s^{-1}, with pronounced spatial variability across the domain, consistent with the heterogeneous MCS occurrence patterns shown in Figure 6. A large fraction of MCSs exhibit westward propagation, indicating a dominant directional preference. Specifically, 25.1% of the systems move westward, followed by 20.3% moving southwest, and 14.8% moving northwestward. This prevalence of westward and southwestward motions aligns with the dominant monsoonal steering flow over central India during JJAS. Zonal analysis reveals that westward-propagating MCSs are slightly more frequent and tend to move faster than eastward propagating systems. The mean speed for westward-moving systems is approximately 6.7 m s^{-1}, compared to 5.8 m s^{-1} for eastward-moving systems. In the meridional direction, southward-propagating MCSs are slightly more frequent and exhibit slightly higher speeds compared to

northward moving systems. The mean speed for southward-propagating systems is 5.7 m s^{-1}, while northward-moving systems propagate at an average of 5.5 m s^{-1}. These propagation characteristics help explain the spatial rainfall patterns presented in section 3.3.1, as regions aligned with the dominant westward and southwestward MCS tracks are more likely to experience frequent MCS passage and enhanced rainfall accumulation.

3.4 Lifecycle evolution storms

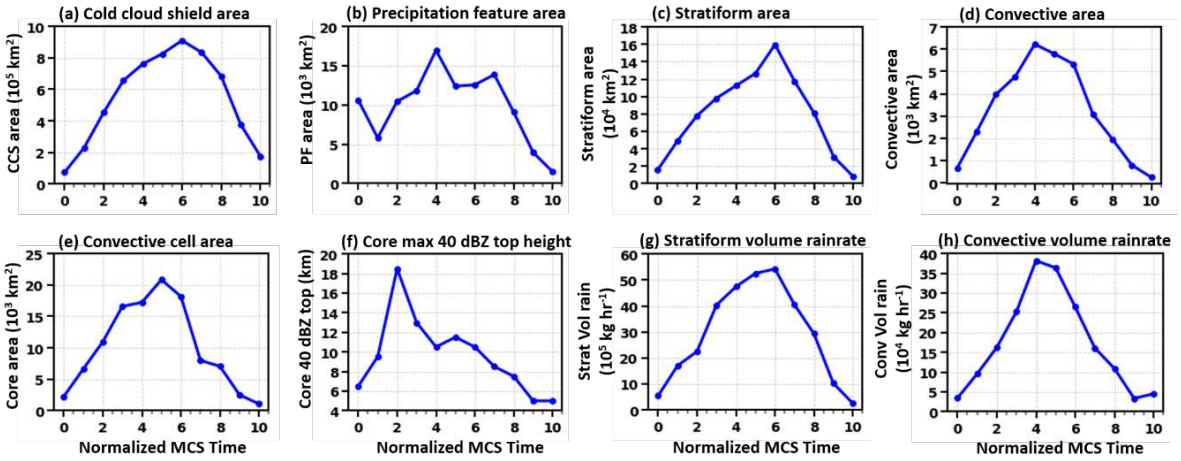


Figure 8: Composite lifecycle evolution of MCS (a) Cold cloud shield area, (b) largest precipitation feature area, (c) Stratiform area, (d) Convective area (e) Convective cell area (f) maximum 40-dBZ echo-top height (g) convective volumetric rain rate, and (h) stratiform volumetric rain rate. MCS lifetimes are normalized between 0 and 1, where 0 denotes convective initiation and 10 denotes dissipation.

The composite lifecycle evolution of MCSs and their embedded storm characteristics derived from radar observations is presented in Figure 8. Ground-based radar data provides a key advantage by capturing the three-dimensional internal structure of MCSs as they evolve and propagate across the radar domain. Given the wide variability in MCS lifetimes, all systems are composited by normalizing their lifecycles to a common scale between 0 and 10, where 0 represents convective initiation and 10 denotes system dissipation, following Feng et al., 2018. This normalization enables a consistent comparison of MCS properties across different systems and lifecycle stages. The first half of the normalized lifecycle broadly corresponds to the growth and organizational phase, while the second half represents system maturity and decay. The CCS area and the largest PF area (Figures 8a and 8b) exhibit a steady increase during the first half of the lifecycle, reaching maximum values during the mature phase (60% of the normalized timeline).

This growth reflects the upscale aggregation of convective elements into a coherent mesoscale structure, consistent with findings from Feng et al., (2018, 2019). Following the mature phase, both CCS and PF areas decrease rapidly, indicating the weakening and eventual dissipation of the system. The evolution of stratiform and convective areas (Figures 8c and 8d), classified using the reflectivity texture-based technique from Steiner et al., (1995), show distinct evolution. Convective areas are considerably smaller in spatial extent and peak earlier in the lifecycle, around 40%, coinciding with the period of strongest convective activity. In contrast, stratiform areas continue to expand beyond the convective peak and reach their maximum extent later, around 60% of the normalized lifetime. This temporal offset reflects the typical evolution of MCSs, where intense deep convection initiates system growth, followed by development of extensive stratiform precipitation as the system matures (Houze, 2004; Parker & Johnson, 2000). On average, the stratiform region spans an area of approximately 7.9×10^4 km^2, whereas the convective region occupies only about 3.2×10^3 km^2 highlighting the dominance of stratiform precipitation in terms of spatial coverage. This extensive stratiform area explains the strong contribution of MCSs to seasonal rainfall totals and provides a physical link to the spatial correspondence between MCS occurrence and accumulated precipitation discussed in Section 3.3.1. The evolution of the largest convective cell area and the maximum 40-dBZ echo-top height (Figures 8e and 8f) provides additional insight into the intensity of embedded convection. Both parameters peak early in the lifecycle, around 20% of the normalized timeline, indicating that the most intense and vertically developed convective cores occur during the initial upscale growth phase. The presence of 40 dBZ reflectivity at elevated altitudes suggests strong updrafts capable of lofting large hydrometeors such as graupel and hail into the upper troposphere (Feng et al., 2018). These early intense convective features play a critical role in organizing the system and initiating the development of extensive stratiform precipitation regions. The volumetric rain rate evolution (Figures 8g and 8h), measure of the total rainfall production from convective and stratiform region further illustrates the transition from convective to stratiform rainfall dominance over the MCS lifecycle. Convective volumetric rain rates peak during the early-to-mid stages of the lifecycle (around 40% of the normalized lifetime). In contrast, stratiform volumetric rain rates peak later and remain elevated for a longer duration during the mature stage, contributing approximately an order of magnitude more rainfall than convective precipitation during that period. This result underscores the critical role of stratiform precipitation in contributing to the total rainfall budget of MCSs, due to both its larger area and sustained precipitation rates.

3.5 Statistical Characterization of Structural Properties of MCS and storms

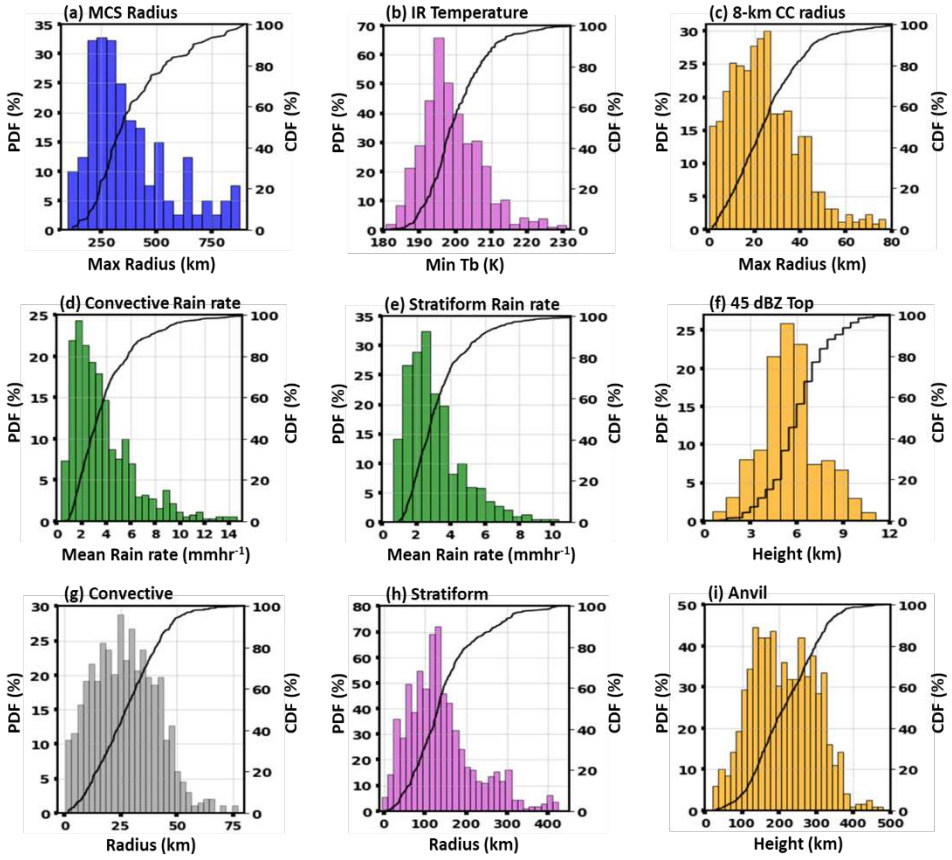


Figure 9: PDF (bars) and CDF (black lines) of (a) maximum size for each tracked MCS, (b) minimum IR temperature, (c) Radius of reflectivity greater than 30 dBZ area at 8 km height, (d) Mean convective rain rate, (e) Mean Stratiform rain rate, (f) 45 dBZ echo top height, and Radius of (g) convective cloud, (h) Stratiform cloud, (i) Anvil cloud of all observed MCS over study domain.

To characterize the morphology and intensity of MCSs throughout their lifecycles, Probability Density Functions (PDFs) and Cumulative Distribution Functions (CDFs) of key structural and microphysical properties are analyzed for all tracked systems over the study domain. The frequency distribution of MCS lifetime (not shown) over the domain shows a population of short as well as long-lived systems. Short-lived MCSs (less than 10 hours) represent the majority (53%), followed by medium-lived (10–20 hours, 27%) and long-lived systems (>30 hours, 21%). Panel (a) shows the distribution of maximum equivalent radius for each tracked MCS. The mean radius is approximately 400 km, with about 63% of MCSs exhibiting radius smaller than 400 km, while 37% extend beyond this threshold. This distribution indicates that

although many MCSs remain moderately sized, a substantial fraction grows into large, expansive systems capable of influencing precipitation over wide areas, consistent with their dominant contribution to seasonal rainfall discussed in Section 3.3.1. The minimum IR brightness temperature distribution (Figure 9b) reveals that approximately 56% of MCSs reach temperatures below 200 K, signifying deep convective cloud tops typical of intense updrafts. These colder temperatures often correspond to overshooting tops and strong vertical development. Figure 9c displays the equivalent radius of reflectivity exceeding 30 dBZ area at 8 km altitude which is a proxy for the horizontal extent of intense convective cores (Rickenbach et al., 2008). The distribution is strongly skewed toward smaller radii, with a pronounced peak around 20-25 km and a rapid decline at larger values. This indicates that while broad cores are possible, most MCSs contain relatively compact regions of strong upper-level reflectivity, a feature commonly associated with vigorous deep convection and strong updrafts (Zipser et al., 2006). The distribution of mean convective and stratiform rain rates (Figures 9d and 9e) exhibit broadly similar distribution but differ in magnitude. Convective rain rates are substantially higher, with a 90th percentile exceeding 8 mm hr^{-1}, whereas stratiform rain rates peak around 5 mm hr^{-1}. This contrast highlights the fundamental difference between the localized high intensity rainfall produced by convective cores and the more widespread but moderate precipitation characteristic of stratiform regions. These rainfall characteristics are essential for evaluating MCS contributions to regional hydrological budgets. The vertical structure of convection is further characterized using the maximum height of the 45 dBZ echo top (Figure 9f), a recognized proxy for strong convective updrafts (Zipser et al., 2006). A distribution exhibits a modal value near 6 km, with the 90^{th} percentile reaching approximately 8.5 km. Such heights suggest that many MCSs contain deep convective towers with potential for hail formation and elevated lightning activity (Williams et al., 1991; Zipser et al., 2006).

Figures 8g–i show the equivalent radii of convective, stratiform, and anvil cloud regions, respectively. Stratiform regions occur more frequently and are generally broader than convective cores, occupying on average about 34% of the area, compared to 17 % for convective regions. However, anvil clouds dominate the spatial footprint, with the distribution extending far beyond that of stratiform and convective regions, particularly at the higher percentiles. At the 90th percentile, anvil cloud area is significantly larger than that of stratiform and convective regions, underscoring their extensive horizontal extent. These results highlight the broad structural and microphysical characteristics of MCSs, particularly emphasizing the extensive spatial footprint of anvil clouds. The large spatial extent of anvil clouds suggests a potentially important role in shaping the upper-level cloud field. To explore this role within MCSs, we examine how anvil cloud radius relates to key storm properties, including convective and stratiform cloud sizes, rain rates, and echo-top heights (Figure 9). Panels (a) and (b) show that the anvil cloud radius exhibits a moderate correlation with convective cloud radius ($r = 0.49$) and a stronger correlation with stratiform cloud radius ($r = 0.75$),

highlighting the influence of stratiform regions on anvil cloud development. This stronger correlation between anvil and stratiform regions aligns with the contiguous nature of stratiform precipitation and the generally broader spatial coverage of stratiform clouds relative to convective cores.

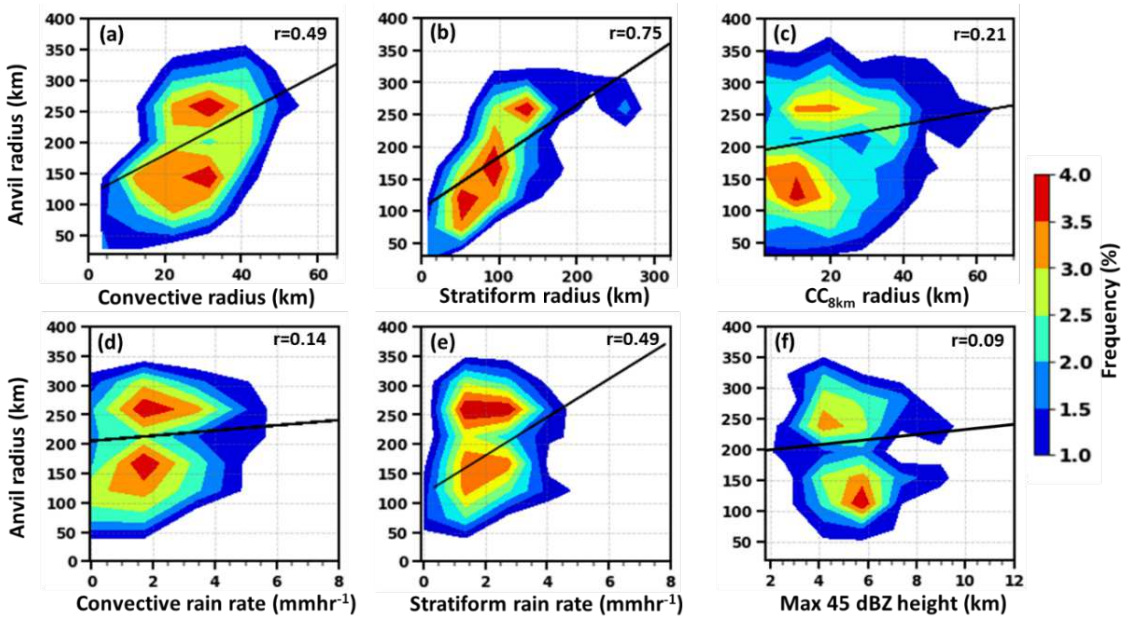


Figure 10: Frequency distribution of the anvil cloud radius as a function of (a) Convective radius, (b) Stratiform radius (c) Radius of 30 dBZ reflectivity area of convective cloud at 8 km height (d) Convective rain rate, and (e) Stratiform rain rate (f) 45 dBZ echo top height of all observed MCS over study domain. The dashed line is the linear fit line from all raw samples, and r is the correlation coefficient.

Stratiform clouds typically produce widespread, relatively lighter precipitation but occupy an extensive horizontal area, providing a contiguous environment that supports the horizontal spreading of ice and mixed-phase hydrometeors that form the anvil cloud. This relationship is further supported by elevated stratiform rain rates observed in Figure 10e and 9e, underscoring the critical role of stratiform regions in the development and spatial extent of trailing anvil cloud structures within MCSs (Cetrone & Houze, 2011; Houze, 1997). Comparative studies utilizing TRMM precipitation radar data have reported similar correlations between anvil and convective cloud radius. For instance, Li & Schumacher, (2011) documented an r-value of 0.50, which supports the robustness of this linkage. In contrast, correlations between anvil radius and parameters indicative of intense convective activity such as the radius of the 30 dBZ reflectivity area at 8 km altitude (Figure 10c), the maximum 45 dBZ echo top height (Figure 6f), and convective rain rate (Figure 10d) are substantially weaker. These results suggest that while convective core size and updraft

strength are reliable indicators of localized storm intensity, they exert limited control over the horizontal extent of the anvil cloud. The formation and spread of the anvil cloud are predominantly governed by stratiform and transitional microphysical processes that facilitate widespread horizontal transport of ice-phase hydrometeors, rather than by the more localized, vertically intense convective cores (Zipser et al., 2006; Li & Schumacher, 2011). Transitional anvils contribute the majority (54%) of the total anvil area, followed by mixed-phase anvils at 30% and ice anvils at 16%. The dominance of transitional anvils, which consist of larger hydrometeor particles and are closely linked to both convective and stratiform areas, which may explain their dominant spatial coverage.

3.6 Diurnal cycle

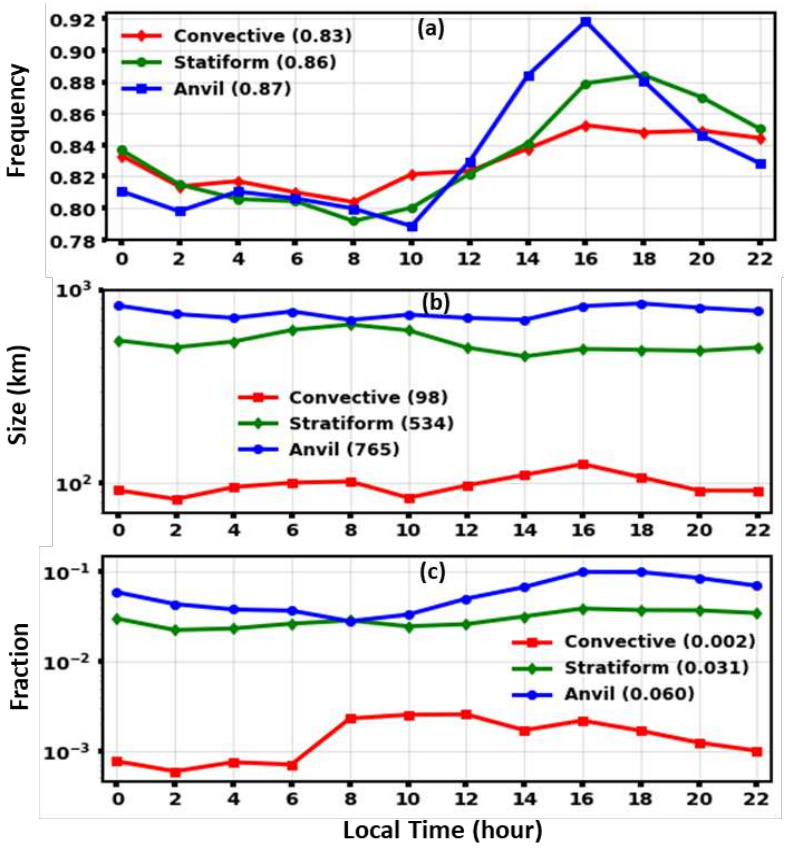


Figure 11: Hourly mean diurnal cycle of Convective (red), stratiform (green) and anvil (blue) cloud over the study domain, (a) Frequency of occurrence, (b) Size (c) areal coverage. Values in the parentheses are average values over the study domain

The diurnal variability of MCS echoes provides insight into the timing and evolution of convective, stratiform, and anvil cloud components. To quantify this behavior, we analyzed the hourly mean diurnal cycle of these echo types across the study domain (Figure 11). The frequency of occurrence (Figure 11a) is defined as the ratio of number of observations for each echo type relative to the total number of available observations within the study domain at each hour. All three echo types exhibit a similar diurnal pattern, their frequencies decrease continuously from midnight to late morning, then rise to peak in the afternoon around 16-18 LT. This behavior aligns with enhanced solar heating and increased boundary layer mixing during the afternoon, which favor convection initiation. These findings are consistent with Carbone et al. (2002), indicating that most MCSs tend to initiate between early and mid-afternoon. The increased frequency of occurrence in the afternoon hours corresponds to the development of small, isolated convective cells, as reflected in their average MCS sizes (Figure 11 b). The anvil cloud area reaches its minimum near 0800 LT and subsequently increases by around 11% relative to this minimum, peaking at approximately 1.8×10^7 km² near 1800 LT. Stratiform cloud regions exhibit their maximum size later, around 2000 LT, before gradually declining through the night. This growth in stratiform area is associated with the organization of individual convective systems into full MCSs during the late afternoon and evening hours, promoting the development of stratiform precipitation (Houze, 2004). Figure 11c illustrates the domain fraction (frequency × areal coverage) captures both how often temporal extent and how broadly spatial extent of each echo type occurs, providing a measure of its overall spatiotemporal dominance in the domain. For convective and stratiform clouds, domain fraction closely follows the pattern of frequency, since their areal coverage remains relatively stable throughout the day (not shown). Convective domain fraction peaks earlier (~08–12 LT), whereas stratiform and anvil domain fractions peak later (~16–18 LT), indicating a time lag between convective initiation and the development of broader MCS structures. This lag reflects the typical MCS lifecycle, where isolated convective cells evolve into organized systems with extensive stratiform and anvil regions. The pronounced dominance of anvil clouds in terms of both areal coverage and domain fraction highlights their significant role in the mature phase of MCSs, particularly in the upper troposphere.

3.7 Storm Structure and Statistical Characteristics

3.7.1 Contoured Frequency by Altitude Diagrams (CFADs)

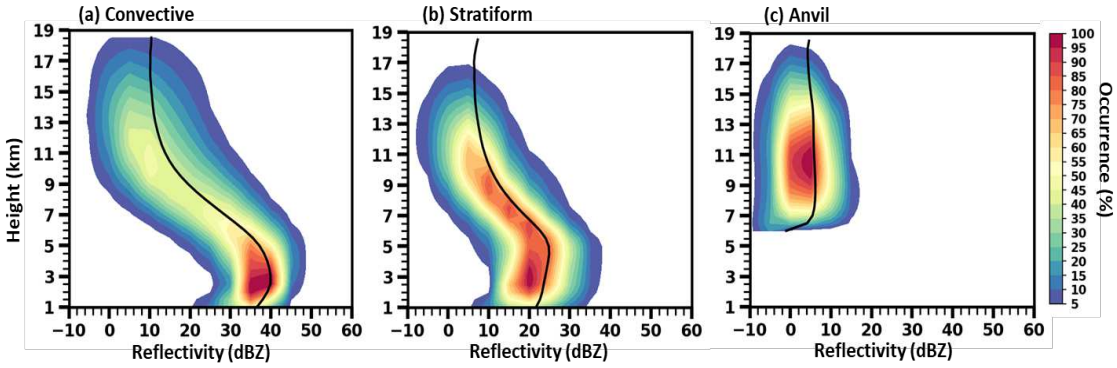


Figure 12. CFADs of radar reflectivity profiles for convective, stratiform, and anvil cloud regions embedded within MCSs over the study domain during JJAS 2019. The black solid line in each panel represents the median reflectivity profile.

To examine the internal vertical structure of convective systems embedded within MCSs, CFADs were employed. CFADs, originally introduced by (Yuter & Houze, 1994), provide a compact way to represent the relative frequency of radar reflectivity at various altitudes and are widely used to investigate storm microphysics and dynamics. In this study, CFADs were constructed using 1012 vertical radar reflectivity profiles from the 2019 monsoon season over the study domain. Reflectivity occurrences between -10 and 60 dBZ were counted in 5 dBZ intervals at each 1 km altitude step from 1 to 18.5 km. These counts were normalized by the maximum frequency across all vertical levels. Vertical levels with reflectivity occurrences less than 10% of the maximum were excluded to ensure statistical robustness. Figure 12 presents the composite CFADs of three dominant cloud types such as convective, stratiform, and anvil identified within MCSs. These cloud types, though part of the same mesoscale system, exhibit distinct vertical reflectivity structures due to differences in their microphysical characteristics and the dynamical environments in which they form. The CFAD for convective clouds (Figure 12 a) exhibits the broadest vertical extent and the highest reflectivity values, with a central mode of 35–40 dBZ concentrated between 1.5 km and 5 km, and a maximum frequency occurring near 3 km altitude. Reflectivity decreases rapidly from 5 to 9 km and a gradual decrease beyond 9 km. Within these levels, several cloud microphysical processes occur, and the resulting reflectivity structure reflects these activities. The broad profile below 5 km suggests the presence of strong updrafts, intense precipitation, and large rain droplets, while the sharp decline aloft indicates the presence of graupel or hail in the mixed-phase region. These hydrometeors require substantial vertical velocities to sustain riming and growth, consistent with vigorous convective

activity (Zipser & Kurt Lutz, 1994; LeMone & Zipser, 1980). In contrast, the stratiform CFAD exhibits a more layered and uniform structure with a strongest reflectivity mode between 15–25 dBZ centered around 3-5 km altitude. Usually, stratiform rain shows a clear increase in reflectivity near 5 km due to melting layer, where ice particles melt into raindrops (Ramana Murty et al., 1965; Konwar et al., 2012; Jha et al., 2019). However, such a pronounced melting-layer signature is not evident in the present CFAD, possibly due to vertical averaging or relatively weak melting-layer contrast. Instead, reflectivity decreases gradually both above and below the peak altitude, indicative of the steady and widespread nature of stratiform precipitation and the absence of strong convective updrafts. The anvil CFAD (Figure 12c) presents a markedly different profile, with negligible reflectivity observed below 5 km and most of the reflectivity confined to the upper troposphere (8-13 km). The highest reflectivity occurs between 9 and 11 km and gradually decreases toward the cloud top, reflecting the detrainment of ice particles from deep convective cores and their lateral spreading to form extensive anvil clouds, consistent with decreasing ice-particle size and number concentration.

3.7.2 Properties of storms Embedded in MCS

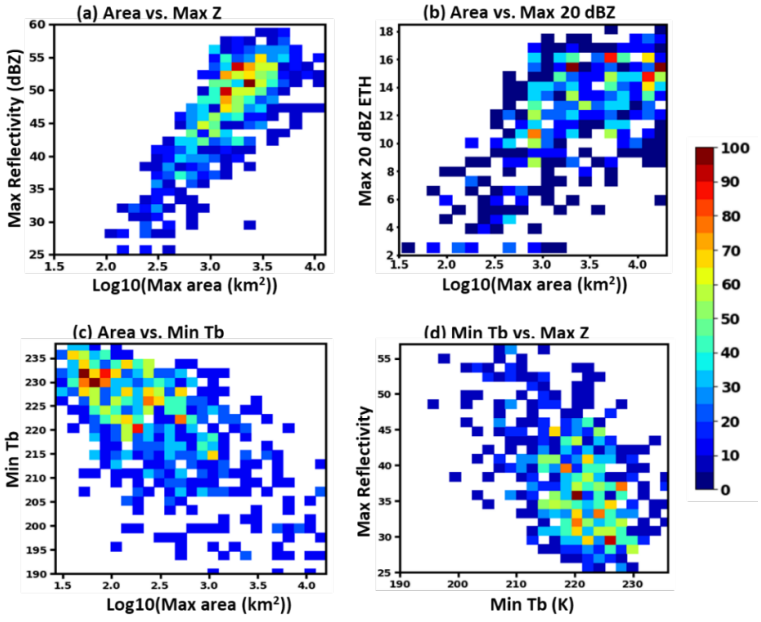


Figure 13. Joint histograms of (a) maximum area and maximum reflectivity, (b) maximum area and maximum 20 dBZ echo-top height, (c) maximum area and minimum brightness temperature (d) minimum brightness temperature and maximum reflectivity of all convective clouds during JJAS 2019 over study domain.

Understanding the structural characteristics of storms embedded within MCSs is crucial for assessing their intensity, organization, and overall contribution to system dynamics. To investigate these features, we analyzed joint histograms of key convective parameters for the JJAS 2019 monsoon season over the study domain. These histograms reveal the relationships between maximum convective cell area, maximum radar reflectivity, 20 dBZ echo-top height, and minimum IR brightness temperature, providing detailed insight into both the horizontal and vertical organization of convection within MCSs (Figure 13). A clear positive relationship between the maximum horizontal area of convective cells and their peak radar reflectivity (Figure 13 a). Larger cells tend to exhibit higher reflectivity values, suggesting that spatially extensive convective systems are generally more intense in terms of precipitation and hydrometeor concentration. The highest frequency occurs for reflectivity values of approximately 45–55 dBZ and cell areas of about 3–3.5 × 10^3 km^2. However, there is a clear tendency for larger cells to exhibit even stronger reflectivity, indicating that broader convective cells often support more vigorous convection. Despite this trend, substantial variability is observed, particularly among smaller cells, which can also exhibit high reflectivity. This indicates that intense convection can also occur in smaller systems. The relationship between the maximum area and the maximum height of the 20 dBZ echo top shown in Figure 13b, reveals a general tendency for larger cells to extend to higher altitudes. Since the 20 dBZ echo-top height serves as a proxy for convective depth, this result suggests that spatially broader cells are, on average, more vertically developed and supported by stronger updrafts. However, echo-top heights vary considerably across all cell sizes, especially for smaller cells, highlighting the variation of convective development. A pronounced inverse relationship is observed between maximum convective cell area and minimum Tb (Figure 13c), with larger cells generally associated with lower Tb values, indicating colder cloud tops and stronger, deeper convection. Many of the largest cells exhibit minimum Tb values below 200 K, supporting the conclusion that broader cells tend to be both more intense and vertically extended. At the same time, several smaller cells also display very low Tb values, highlighting that intense, deep convection can occur across a wide range of spatial scales within MCSs. This variation in convective behavior further illustrates the complex and multi-scale nature of convection within MCSs. The joint histogram of minimum Tb and maximum radar reflectivity (Figure 13d) further confirms the close linkage between convective depth and intensity. Cells with the coldest cloud tops tend to exhibit the highest reflectivity values, frequently exceeding 45–50 dBZ. This inverse relationship reflects the combined influence of strong updrafts, enhanced hydrometeor growth, and efficient precipitation processes in deep convective cores. Notably, for a given Tb, the spread in reflectivity is relatively large, whereas Tb varies less for a given reflectivity. This suggests that while deeper convection is generally more intense, intensity can vary significantly even among cells of similar depth, pointing to the influence of other factors such as microphysical processes or storm dynamics. These findings show that both large and small convective cells contribute substantially to intense

rainfall and deep convection during the monsoon season, highlighting the multi-scale nature of convective organization within MCSs. Building on the relationships between convective scale, depth, and intensity identified in Figure 13, we next examine how the large-scale environment influences anvil cloud size and the evolution of MCSs

3.7.3 Environmental Influences on Size and Lifetime in MCSs

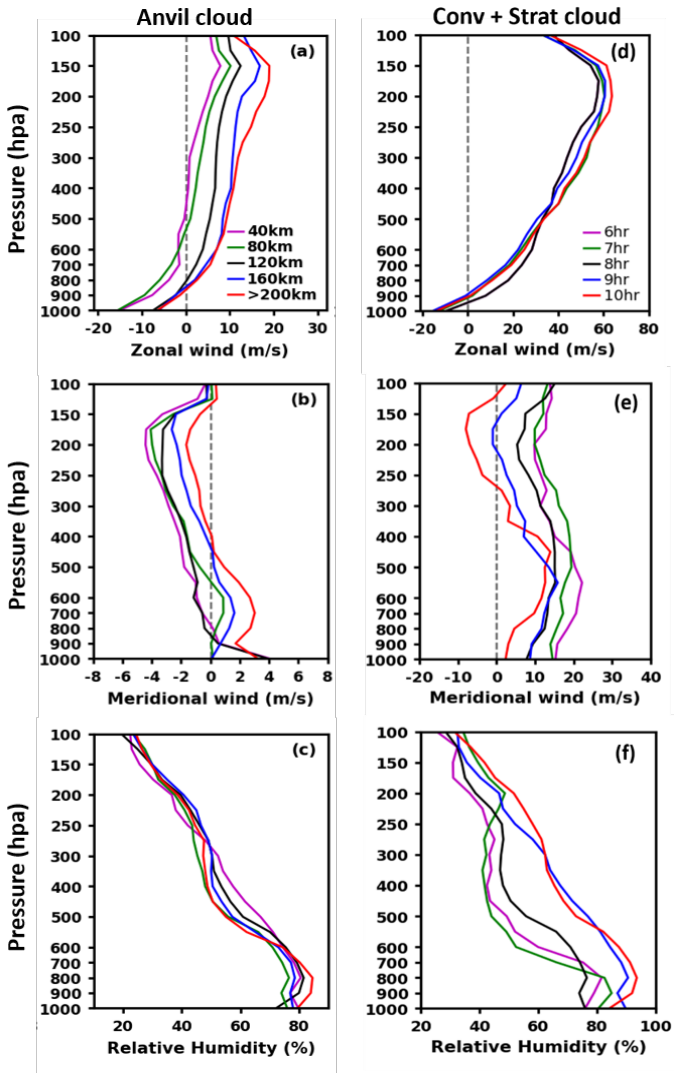


Figure 14. Composite vertical profiles of zonal wind, meridional wind, and relative humidity stratified by anvil cloud radius (a–c) and system lifetime (d–f) during developing and mature stages of MCSs, with lifetime composites separated into convective and stratiform regions.

To assess the environmental controls on anvil cloud development and MCS longevity, composite vertical profiles of atmospheric state variables from ERA5 were analyzed and are now presented together in a unified framework. Figure 14 (a–c) show profiles stratified by maximum anvil cloud radius, while Figure 14 (d–f) show profiles composited by system lifetime (6–10 h), averaged over convective and stratiform rain regions. In this analysis, MCSs are classified into anvil-size categories based on the maximum anvil cloud radius attained during their lifetime, and into lifetime categories according to their total duration from initiation to dissipation. The wind structure reveals a clear dependence of anvil extent on the upper-tropospheric flow. As shown in Figure 14 (a), zonal wind speeds in the upper troposphere (150–200 hPa) increase systematically with anvil radius. Systems with largest anvils (>200 km) exhibit mean zonal wind speeds of approximately 18.4 m s^{-1}, representing about a 27% increase compared to systems with anvil radii near 40 km. This behavior indicates that stronger upper-level flow and enhanced deep-layer wind shear favor the lateral spreading and maintenance of extensive anvil clouds. In contrast, the meridional wind profiles (Figure 14 b) show a weaker and less coherent dependence on anvil size. Although the differences are modest, larger-anvil systems exhibit slightly stronger upper-tropospheric meridional winds and a greater vertical contrast between upper and lower-tropospheric flow, indicating enhanced directional shear in environments that support broader anvils. However, this signal remains weaker than that of the zonal wind, suggesting that anvil expansion is more strongly controlled by the dominant large-scale zonal flow during the monsoon season. Relative humidity (Figure 14 c) exhibits relatively small differences in the upper troposphere across anvil-size categories. However, notable contrasts appear in the mid-troposphere (300–600 hPa), where larger-anvil systems tend to have slightly lower RH compared to smaller-anvil systems. This is likely to reflect sampling differences, smaller anvils are more closely associated with active convective cores and stratiform regions, whereas larger anvils extend farther from the convective source and increasingly incorporate drier environmental air. In contrast to anvil size, system lifetime shows a different set of environmental sensitivities (Figure 14 d–f). Zonal winds (Figure 14d) increase with height but display little variation across lifetime categories, indicating a limited role in governing MCS longevity. Meridional winds (Figure 14 e), however, show a clearer dependence, longer-lived systems (9–10 h) exhibit stronger deep-layer meridional shear compared to shorter-lived systems (6–7 h). This suggests that enhanced directional shear contributes to improved convective organization and persistence. The strongest thermodynamic control on lifetime is seen in relative humidity (Figure 14f). Longer-lived systems (9-10 h) maintain higher mid-tropospheric moisture (approximately 250–700 hPa), whereas shorter-lived systems are embedded in comparatively drier environments. High mid-level humidity reduces entrainment of dry air into convective updrafts, limiting their weakening and supporting sustained stratiform precipitation. This moisture-rich environment is therefore a key factor in promoting longer system duration. The dynamical and thermodynamic characteristics indicate a clear distinction between the

controls on anvil size and system longevity. Anvil expansion is primarily regulated by upper-tropospheric zonal flow and associated shear, whereas MCS lifetime is more strongly influenced by mid-level moisture availability and deep-layer meridional shear. Together, these factors support convective organization and enhance system persistence.

4. Conclusion and Future Scope:

This study provides a comprehensive observational characterization of MCSs and their embedded storm structures over the core monsoon zone during the 2019 summer monsoon. Using high-resolution satellite and radar observations, the study highlights the typical lifecycle of MCSs from convective initiation to mature and dissipation stages, characterized by deep convection, expanding stratiform regions, and extensive anvil clouds. The evolution of cloud structures, precipitation features, and convective intensity confirms the classical behavior of MCSs in the monsoon environment. The integration of classification-based tracking techniques with radar and satellite data demonstrates an effective approach for understanding storm-scale dynamics within MCSs. These insights are crucial for improving prediction of extreme rainfall and severe weather over Central India, where monsoon convection plays a dominant role in the regional climate.

The key findings of this study are summarized as follows:

- A total of 93 MCSs were tracked over the Bhopal radar domain, contributing more than 40% of seasonal rainfall. Their predominantly westward propagation, (mean speed ~9.1 m s^{-1}), plays a key role in shaping rainfall distribution and associated flood risk.
- MCS evolution is characterized by an early phase of intense, vertically developed convective cores, followed by the expansion of stratiform and anvil regions. While convection dominates rainfall intensity, stratiform precipitation contributes most volumetric rainfall due to its larger spatial extent and persistence, highlighting the need to accurately represent 3D storm structure in observations and models.
- The structural organization of MCSs showing the anvil extent is more strongly linked to stratiform regions ($r = 0.75$) than to convective cores ($r = 0.49$), underscoring the dominant role of stratiform processes in controlling system-scale cloud structure and precipitation distribution.
- A pronounced diurnal cycle is observed, with convective activity peaking during the afternoon and transitioning to stratiform and anvil-dominated structures in the evening. This reflects the typical upscale growth of convection into organized MCS.

- CFAD analysis reveals distinct vertical signatures of convective, stratiform, and anvil regions, indicating strong updraft-driven deep convection, layered stratiform precipitation, and upper-tropospheric ice-dominated anvils, respectively, highlighting the vertically stratified nature of MCS evolution.
- Convective cells exhibit strong variability across scales; larger cells tend to be deeper and more intense, but smaller cells can also produce strong convection, emphasizing the multi-scale nature of convective processes within MCSs.
- Environmental analysis indicates that larger anvils are favored by stronger deep-layer shear and higher mid-level moisture, which promotes organized convection, stratiform persistence, and enhanced anvil expansion, thereby increasing MCS structural organization and longevity.

The findings of this study provide an important observational benchmark for evaluating high-resolution numerical models and improving representation of convective organization in monsoon environments. Future work should focus on extending this analysis to multiple monsoon seasons to assess interannual variability and the influence of large-scale modes of variability. In addition, integrating dual-polarimetric radar observations and cloud-resolving model simulations would help to further elucidate microphysical processes governing stratiform and anvil formation. Improved understanding of storm-scale dynamics within MCSs will ultimately enhance predictive capability for extreme rainfall events and associated hydrological hazards over the Indian monsoon region.

Acknowledgments

Indian Institute of Tropical Meteorology (IITM) is funded by the Ministry of Earth Sciences (MoES), Government of India. Authors acknowledge the support from the Director, IITM, for pursuing the research. Manisha Tupsoundare is supported by the IITM Research Fellowship and this work is part of her PhD thesis. Zhe Feng is supported by US Department of Energy Office of Science Biological and Environmental Research (BER) as part of the Regional and Global Modeling Analysis (RGMA) program area through the Water Cycle and Climate Extremes Modeling (WACCEM) scientific focus area. Pacific Northwest National Laboratory is operated for DOE by the Battelle Memorial Institute under contract DE-AC05-76RL01830.

Data Availability Statement

In this study, the ERA5 reanalysis data is available from the Copernicus Climate Change Service Climate Data Store (https://doi.org/10.24381/cds.bd0915c6 and https://doi.org/10.24381/cds.adbb2d47), after registration. The brightness temperature data are obtained from the NASA Goddard Earth Sciences Data and Information Services Center (GES DISC) Global Precipitation Measurement (GPM) MERGIR dataset (https://disc.gsfc.nasa.gov/datasets/GPM_MERGIR_1/summary). Precipitation data are sourced from the GPM Integrated Multi-satellite Retrievals for GPM (IMERG) Final Run half-hourly dataset (https://disc.gsfc.nasa.gov/datasets/GPM_3IMERGHH_07/summary). The PyFLEXTRKR tracking codes can be found on GitHub (Feng et al., 2023). The radar and MCS data used in this study are stored at the Atmospheric Research Data Center (ARDC) of Indian Institute of Tropical Meteorology and can be accessed via FTP/SFTP at 10.119.14.33:/2PB_DDNStorage/gpfs_adl/ART upon request from the corresponding author for research collaboration. Additionally, Global track data sets of monsoon low-pressure systems (LPSs) are accessible from (Vishnu et al., 2020). The topography data (Global 30 Arc-Second Elevation [GTOPO30]) were obtained from the U.S. Geological Survey: https://doi.org/10.5066/F7DF6PQS.

Declarations

Conflict of Interest Statement: The authors declare no competing interests.

References

Cetrone, J., & Houze, R. A. (2006). Characteristics of Tropical Convection over the Ocean near Kwajalein. *Monthly Weather Review*.

Cetrone, J., & Houze, R. A. (2011). Leading and trailing anvil clouds of West African squall lines. *Journal of the Atmospheric Sciences*, *68*(5), 1114–1123. https://doi.org/10.1175/2011JAS3580.1

Coniglio, M. C., Stensrud, D. J., & Wicker, L. J. (2006). *Effects of Upper-Level Shear on the Structure and Maintenance of Strong Quasi-Linear Mesoscale Convective Systems*.

Das, S. K., Hazra, A., Deshpande, S. M., Krishna, U. V. M., & Kolte, Y. K. (2021). Investigation of Cloud Microphysical Features During the Passage of a Tropical Mesoscale Convective System: Numerical Simulations and X-Band Radar Observations. *Pure and Applied Geophysics*, *178*(1), 185–204. https://doi.org/10.1007/s00024-020-02622-w

905 Davini, P., Bechini, R., Cremonini, R., & Cassardo, C. (2011). Radar-based analysis of convective storms
906 over Northwestern italy. *Atmosphere*, *3*(1), 33–58. https://doi.org/10.3390/atmos3010033

907 Deshpande, S. M., Dhangar, N., Das, S. K., Kalapureddy, M. C. R., Chakravarty, K., Sonbawne, S., &
908 Konwar, M. (2015). Mesoscale kinematics derived from X-band Doppler radar observations of
909 convective versus stratiform precipitation and comparison with GPS radiosonde profiles. *Journal of*
910 *Geophysical Research*, *120*(22), 11,536-11,551. https://doi.org/10.1002/2014JD022595

911 Dixon Michael. (1993). TITAN Thunderstorm Identification, Tracking, Analysis, and Nowcasting. *Journal*
912 *of Atmospheric and Oceanic Technology*.

913 Dixon M. EOL/RAL, cited 2014. Radx C++ software package for radial radar data. [Available online at
914 htttp://www.ral.ucar.edu/projects/titan/docs/radial_formats/radx .html.].

915 Doswell Iii, C. A., Brooks, H. E., & Maddox, R. A. (1996). Flash Flood Forecasting: An Ingredients-Based
916 Methodology. *Weather and Forecasting*.

917 Doyle, A., Stein, T., & Turner, A. (2021). Temporal patterns in radar-observed convective cell development
918 during the 2016 monsoon onset. *Weather*, *76*(6), 180–184. https://doi.org/10.1002/wea.3969

919 Feng, Z., Dong, X., Xi, B., Schumacher, C., Minnis, P., & Khaiyer, M. (2011). Top-of-atmosphere radiation
920 budget of convective core/stratiform rain and anvil clouds from deep convective systems. *Journal of*
921 *Geophysical Research Atmospheres*, *116*(23). https://doi.org/10.1029/2011JD016451

922 Feng, Z., Hardin, J., Barnes, H. C., Li, J., Leung, L. R., Varble, A., & Zhang, Z. (2023). PyFLEXTRKR: a
923 flexible feature tracking Python software for convective cloud analysis. *Geoscientific Model*
924 *Development*, *16*(10), 2753–2776. https://doi.org/10.5194/gmd-16-2753-2023

925 Feng, Z., Houze, R. A., Leung, L. R., Hardin, J. C., Jingyu Wang, William Gustafson, & Homeyer, C. R.
926 (2019). Spatiotemporal Characteristics and Large-Scale Environments of Mesoscale Convective
927 Systems East of the Rocky Mountains. *Journal of Geophysical Research: Atmospheres*.
928 https://doi.org/10.1175/JCLI-D-19

929 Feng, Z., Leung, L. R., Hagos, S., Houze, R. A., Burleyson, C. D., & Balaguru, K. (2016). More frequent
930 intense and long-lived storms dominate the springtime trend in central US rainfall. *Nature*
931 *Communications*, *7*. https://doi.org/10.1038/ncomms13429

932 Feng, Z., Leung, L. R., Houze, R. A., Hagos, S., Hardin, J., Yang, Q., Han, B., & Fan, J. (2018). Structure
933 and Evolution of Mesoscale Convective Systems: Sensitivity to Cloud Microphysics in Convection-

Permitting Simulations Over the United States. *Journal of Advances in Modeling Earth Systems*, *10*(7), 1470–1494. https://doi.org/10.1029/2018MS001305

Futyan, J. M., and A. D. Del Genio (2007), Deep convective system evolution over Africa and the Tropical Atlantic, J. Clim., 20(20), 5041–5060, doi:10.1175/JCLI4297.1

Goudenhoofdt, E., & Delobbe, L. (2013). Statistical characteristics of convective storms in belgium derived from volumetric weather radar observations. *Journal of Applied Meteorology and Climatology*, *52*(4), 918–934. https://doi.org/10.1175/JAMC-D-12-079.1

Houze, R. A. (1977). Houze 1977 Structure and dynamics of a tropical squall-line system. *Monthly Weather Review*.

Houze, R. A. (1989). Observed structure of mesoscale convective systems and implications for large-scale heating. In *No. 487 Q. 1. R. Mefeorol. SOC* (Vol. 115).

Houze, R. A. (1997). Stratiform Precipitation in Regions of Convection A Meteorological Paradox. *American Meteorological Society*.

Houze, R. A. (2004). Mesoscale convective systems. In *Reviews of Geophysics* (Vol. 42, Number 4, pp. 1–43). https://doi.org/10.1029/2004RG000150

Houze, R. A. (2018). 100 Years of Research on Mesoscale Convective Systems. *Meteorological Monographs*, *59*, 17.1-17.54. https://doi.org/10.1175/amsmonographs-d-18-0001.1

Houze, R. A., & Betts. (1981). Convection in GATE. *Reviews of Geophysics and Space Physics*.

Houze, R. A., & Mapes, B. (1991, May). Oceanic mesoscale convective systems of the Australian monsoon. *19th Conference on Hurricanes & Tropical Meteorology*.

Houze, R. A., Rasmussen, K. L., Zuluaga, M. D., & Brodzik, S. R. (2015). The variable nature of convection in the tropics and subtropics: A legacy of 16 years of the Tropical Rainfall Measuring Mission satellite. In *Reviews of Geophysics* (Vol. 53, Number 3, pp. 994–1021). Blackwell Publishing Ltd. https://doi.org/10.1002/2015RG000488

Hu, H., Leung, L. R., & Feng, Z. (2021). Early warm-season mesoscale convective systems dominate soil moisture-precipitation feedback for summer rainfall in central United States. *Proceedings of the National Academy of Sciences*. https://doi.org/10.1073/pnas.2105260118/-/DCSupplemental

961 Huffman, G. J., Stocker, E. F., Bolvin, D. T., Nelkin, E. J., & Tan, J. (2023). GPM IMERG final
962 precipitation L3 half hourly 0.1 degree x 0.1 degree V07 [Dataset]. *Goddard Earth Sciences Data and*
963 *Information Services Center (GES DISC)*. https://doi.org/10.5067/GPM/IMERG/3BHH/07

964 Janowiak, J., Joyce, B., & Xie, P. (2017). NCEP/CPC L3 half hourly 4km global (60S–60N) merged IR,
965 V1 [Dataset]. *NCEP Climate Prediction Center*. https://doi.org/10.5067/p4hzb9n27eku

966 Jha, A. K., Das, S. K., Deshpande, S. M., & Murali Krishna, U. V. (2023). Radar observed convective storm
967 characteristics at the eastern edge of the Indian summer monsoon trough. *Climate Dynamics*, *61*(7–
968 8), 3633–3652. https://doi.org/10.1007/s00382-023-06759-x

969 Jha, A. K., Kalapureddy, M. C. R., Devisetty, H. K., Deshpande, S. M., & Pandithurai, G. (2019). A case
970 study on large-scale dynamical influence on bright band using cloud radar during the Indian summer
971 monsoon. *Meteorology and Atmospheric Physics*, *131*(3), 505–515. https://doi.org/10.1007/s00703-
972 018-0583-8

973 Konwar, M., Maheskumar, R. S., Das, S. K., & Morwal, S. B. (2012). Nature of light rain during presence
974 and absence of bright band. *Journal of Earth System Science*.

975 Krishna, U. V. M., Das, S. K., Deshpande, S. M., & Pandithurai, G. (2021). Physical processes controlling
976 the diurnal cycle of convective storms in the Western Ghats. *Scientific Reports*, *11*(1).
977 https://doi.org/10.1038/s41598-021-93173-0

978 Kumar, S., & Bhat, G. S. (2016). Vertical profiles of radar reflectivity factor in intense convective clouds
979 in the tropics. *Journal of Applied Meteorology and Climatology*, *55*(5), 1277–1286.
980 https://doi.org/10.1175/JAMC-D-15-0110.1

981 Kumar, S., & Bhat, G. S. (2017). Vertical structure of orographic precipitating clouds observed over south
982 Asia during summer monsoon season. *Journal of Earth System Science*, *126*(8).
983 https://doi.org/10.1007/s12040-017-0897-9

984 Lang, S., Tao, W. K., Cifelli, R., Olson, W., Halverson, J., Rutledge, S., & Simpson, J. (2007). Improving
985 simulations of convective systems from TRMM LBA: Easterly and westerly regimes. *Journal of the*
986 *Atmospheric Sciences*, *64*(4), 1141–1164. https://doi.org/10.1175/JAS3879.1

987 Li, W., & Schumacher, C. (2011). Thick anvils as viewed by the TRMM precipitation radar. *Journal of*
988 *Climate*, *24*(6), 1718–1735. https://doi.org/10.1175/2010JCLI3793.1

Liu, C., Shige, S., Takayabu, Y. N., & Zipser, E. (2015). Latent heating contribution from precipitation systems with different sizes, depths, and intensities in the tropics. *Journal of Climate*, *28*(1), 186–203. https://doi.org/10.1175/JCLI-D-14-00370.1

Liu, N., Leung, L. R., & Feng, Z. (2021). Global Mesoscale Convective System Latent Heating Characteristics from GPM Retrievals and an MCS Tracking Dataset. *Journal of Climate*, *34*(21), 8599–8613. https://doi.org/10.1175/JCLI-D-20-0997.1

Lopez R E. (1976). Radar Characteristics of the Cloud Populations of Tropical Disturbances in the Northwest Atlantic. *Monthly Weather Review*.

Mangla, R., Indu, J., & Lakshmi, V. (2020). Evaluation of convective storms using spaceborne radars over the Indo-Gangetic Plains and western coast of India. *Meteorological Applications*, *27*(3). https://doi.org/10.1002/met.1917

Mapes, B., Tulich, S., Lin, J., & Zuidema, P. (2006). The mesoscale convection life cycle: Building block or prototype for large-scale tropical waves? *Dynamics of Atmospheres and Oceans*, *42*(1–4), 3–29. https://doi.org/10.1016/j.dynatmoce.2006.03.003

LeMone, & Zipser, E. (1980). Cumulonimbus Vertical Velocity Events in GATE. Part I Diameter, Intensity and Mass Flux. *Journal of Atmospheric Sciences*.

May, P. T., & Ballinger, A. (2007). The statistical characteristics of convective cells in a monsoon regime (Darwin, Northern Australia). *Monthly Weather Review*, *135*(1), 82–92. https://doi.org/10.1175/MWR3273.1

Moncrieff, M. W. (1992). Organized Convective Systems: Archetypal Dynamical Models, Mass and Momentum Flux Theory, and Parametrization. *Quarterly Journal of the Royal Meteorological Society*, *118*(507), 819–850. https://doi.org/10.1002/qj.49711850703

Nesbitt, S. W., Cifelli, R., & Rutledge, S. A. (2006). Storm Morphology and Rainfall Characteristics of TRMM Precipitation Features. *Monthly Weather Review*. http://tsdis.gsfc.nasa.gov.

Novo, S., Martínez, D., & Puentes, O. (2013). Tracking, analysis, and nowcasting of cuban convective cells as seen by radar. *Meteorological Applications*, *21*(3), 585–595. https://doi.org/10.1002/met.1380

Parker, M. D., & Johnson, R. H. (2000). Organizational Modes of Midlatitude Mesoscale Convective Systems. *American Meteorological Society*.

Phadtare, J., & Bhat, G. S. (2019). Characteristics of Deep Cloud Systems under Weak and Strong Synoptic Forcing during the Indian Summer Monsoon Season. *Monthly Weather Review*. https://doi.org/10.1175/MWR-D-18

Pokhrel, S., & Sikka, D. R. (2013). Variability of the TRMM-PR total and convective and stratiform rain fractions over the Indian region during the summer monsoon. *Climate Dynamics*, *41*(1), 21–44. https://doi.org/10.1007/s00382-012-1502-1

Potts, R. J., Keenan, T. D., & May, P. T. (2000). Radar Characteristics of Storms in the Sydney Area. *Monthly Weather Review*.

Rajeevan, M., Gadgil, S., & Bhate, J. (2010). Active and break spells of the Indian summer monsoon. *Journal of Earth System Science*.

Ramana Murty, Roy A K, & Biswas K R. (1965). Radar Echo Intensities Below Bright Band. *Journal of Atmospheric Sciences*.

Resmi, E., Malap, N., Kulkarni, G., Murugavel, P., Nair, S., Burger, R., & Prabha, T. V. (2015). Diurnal cycle of convection during the CAIPEEX 2011 experiment. *Theoretical and Applied Climatology*, *126*(1–2), 351–367. https://doi.org/10.1007/s00704-015-1595-7

Rickenbach, T., Ferreira, R. N., Guy, N., & Williams, E. (2008). Radar-observed squall line propagation and the diurnal cycle of convection in Niamey, Niger, during the 2006 African monsoon and multidisciplinary analyses intensive observing period. *Journal of Geophysical Research Atmospheres*, *114*(3). https://doi.org/10.1029/2008JD010871

Roca, R., Aublanc, J., Chambon, P., Fiolleau, T., & Viltard, N. (2014). Robust observational quantification of the contribution of mesoscale convective systems to rainfall in the tropics. *Journal of Climate*, *27*(13), 4952–4958. https://doi.org/10.1175/JCLI-D-13-00628.1

Rowe, A. K., Rutledge, S. A., & Lang, T. J. (2012). Investigation of microphysical processes occurring in organized convection during name. *Monthly Weather Review*, *140*(7), 2167–2187. https://doi.org/10.1175/MWR-D-11-00124.1

Schiro, K. A., Sullivan, S. C., Kuo, Y. H., Su, H., Gentine, P., Elsaesser, G. S., Jiang, J. H., & Neelin, J. D. (2020). Environmental controls on tropical mesoscale convective system precipitation intensity. *Journal of the Atmospheric Sciences*, *77*(12), 4233–4249. https://doi.org/10.1175/JAS-D-20-0111.1

Schumacher, C., & Houze, R. A. (2003). Stratiform Rain in the Tropics as Seen by the TRMM Precipitation Radar *. *American Meteorological Society*. http://daac.gsfc.nasa.gov/;

Schumacher, C., Houze, R. A., & Kraucunas, I. (2004). The Tropical Dynamical Response to Latent Heating Estimates Derived from the TRMM Precipitation Radar. *American Meteorological Society*.

Shah, S., Notarpietro, R., & Branca, M. (2015). Storm identification, tracking and forecasting using high-resolution images of short-range X-band radar. *Atmosphere*, *6*(5), 579–606. https://doi.org/10.3390/atmos6050579

Sindhu, K. D., & Bhat, G. S. (2018). Characteristics of monsoonal precipitating cloud systems over the Indian subcontinent derived from weather radar data. *Quarterly Journal of the Royal Meteorological Society*, *144*(715), 1742–1760. https://doi.org/10.1002/qj.3328

Sindhu, K. D., & Bhat, G. S. (2019). Storm characteristics and precipitation estimates of monsoonal clouds using C-band polarimetric radar over Northwest India. *Theoretical and Applied Climatology*, *138*(1–2), 237–248. https://doi.org/10.1007/s00704-019-02828-6

Sindhu, K. D., & Bhat, G. S. (2021). Seasonal characteristics of storms over the Indian subcontinent. *Scientific Reports*, *11*(1). https://doi.org/10.1038/s41598-021-82237-w

Steiner, Houze, R. A., & Yuter. (1995). Steiner 1995 Climatological Characterization of Three-Dimensional Storm Structure from Operational Radar and Rain Gauge Data. *Journal of Applied Meteorology*.

Tupsoundare, M., Deshpande, S. M., Feng, Z., Das, S. K., Deshpande, M., & Hanmante, H. (2025). Spatiotemporal Variations in the Characteristics of Mesoscale Convective Systems Over Indian Monsoon Zone. *Journal of Geophysical Research: Atmospheres*, *130*(4). https://doi.org/10.1029/2024JD042344

Utsav, B., Deshpande, S. M., Das, S. K., & Pandithurai, G. (2017). Statistical Characteristics of Convective Clouds over the Western Ghats Derived from Weather Radar Observations. *Journal of Geophysical Research: Atmospheres*, *122*(18), 10,050-10,076. https://doi.org/10.1002/2016JD026183

Williams, E. R., Rutledge, S. A., & S.G. Geotis. (1991). A Radar and Electrical Study of Tropical Hot Towers. *Journal of Atmospheric Sciences*.

Yang, Q., & Majda, A. J. (2017). Upscale impact of mesoscale disturbances of tropical convection on synoptic-scale equatorial waves in two-dimensional flows. *Journal of the Atmospheric Sciences*, *74*(9), 3099–3120. https://doi.org/10.1175/JAS-D-17-0068.1

Yang, Q., Ruby, L. L., Feng, Z., & Chen, X. (2023). Impact of Global Warming on U.S. Summertime Mesoscale Convective Systems: A Simple Lagrangian Parcel Model Perspective. *Journal of Climate*, *36*(14), 4597–4618. https://doi.org/10.1175/JCLI-D-22-0291.1

Yuan, J., & Houze, R. A. (2010). Global variability of mesoscale convective system anvil structure from A-train satellite data. *Journal of Climate*, *23*(21), 5864–5888. https://doi.org/10.1175/2010JCLI3671.1

Yuter, & Houze, R. A. (1994). Three-dimensional kinematics and microphysical evolution of Florida cumulonimbus Part II Frequency distributions of vertical velocity, reflectivity, and ZDR. *American Meteorological Society*.

Zipser, E. (1977). Mesoscale and Convective-Scale Downdrafts as Distinct Components of Squall-Line Structure. *Monthly Weather Review*.

Zipser, Cecil, D. J., Liu, C., Nesbitt, S. W., & Yorty, D. P. (2006). WHERE ARE THE MOST. INTENSE THUNDERSTORMS ON EARTH? *American Meteorological Society*. https://doi.org/10.1175/BAMS-87-8-I057

Zipser, E., & Kurt Lutz. (1994). The Vertical Profile of Radar Reflectivity of Convective Cells A Strong Indicator of Storm Intensity and Lightning Probability. *American Meteorological Society*.